Charged current neutrino interactions in hot and dense matter

Luke F. Roberts and Sanjay Reddy

Phys. Rev. C **95**, 045807 — Published 27 April 2017

DOI: 10.1103/PhysRevC.95.045807

INT-PUB-16-048

Charged current neutrino interactions in hot and dense matter

Luke F. Roberts[1] and Sanjay Reddy[2]

[1] *National Superconducting Cyclotron Laboratory and Department of Physics and Astronomy, Michigan State University, East Lansing, Michigan 48824, USA**

[2] *Institute for Nuclear Theory, University of Washington, Seattle, Washington 98195, USA*†

We derive the charged current absorption rate of electron and anti-electron neutrinos in dense matter using a fully relativistic approach valid at arbitrary matter degeneracy. We include mean field energy shifts due to nuclear interactions and the corrections due to weak magnetism. The rates are derived both from the familiar Fermi's Golden Rule, and from the techniques of finite temperature field theory, and shown to be equivalent. In various limits, these results can also be used to calculate neutral current opacities. We find that some pieces of the response have been left out in previous derivations and their contribution at high density can be significant. Useful formulae and detailed derivations are presented and we provide a new open source implementation of these opacities for use in radiation hydrodynamic simulations of core-collapse supernovae and neutron star mergers.

I. INTRODUCTION

Neutrino opacities in dense matter are of paramount importance to the evolution of core-collapse supernovae and the remnants of compact object mergers. They impact the properties of the neutrino signal of these events [e.g. 1, 2], are integral to the rate of energy transport [e.g. 3], and can strongly alter the composition of matter ejected in these events [e.g. 4, 5]. Recent work on modeling core-collapse supernovae has shown that three-dimensional models are close to explosion, but the results are sensitive to small changes in the neutrino opacities and other simulation inputs [6–9]. Therefore, it is important to provide accurate expressions for the neutrino opacities required for these numerical models.

In dense matter many-body effects can modify the neutrino mean free paths. The inclusion of the nucleon self energies and effective masses in the medium can significantly alter electron neutrino and anti-neutrino emission. These effects were first realized in [10] and have been the focus of recent work because of its implications for neutrino spectra and nucleosynthesis [11–15]. In addition, earlier studies have shown that neutrino interactions in dense matter are influenced by matter degeneracy, and strong and electromagnetic correlations between nucleons and leptons in the dense medium [16–21]. These effects can suppress the neutrino opacity at and above nuclear saturation density [19, 20, 22] and significantly accelerate protoneutron star cooling at late times [2, 23]. Multi-particle excitations [13, 24] and coherent scattering from a mixed phase [25–27] may also strongly impact neutrino interaction rates and neutrino emission in supernovae. The strength of all of these effects depend on the assumed form of the nuclear interaction which also influences the nuclear equation of state (EoS). These effects on the EoS and neutrino opacities are correlated [16–21] and they should be calculated from the same nuclear interaction.

Charged current neutrino interaction rates, such as $\nu_e + n \rightarrow e^- + p$ are particularly sensitive to changes in the dispersion relations of nucleons because the potential energy difference between the proton and neutron can alter the lepton kinematics, which are often frustrated by final state blocking due to degeneracy [10, 11, 13, 15]. Although there has been significant focus on including these effects in neutrino interaction rates, there is still no complete, relativistic formalism available. The work of [21] completely neglects the impact of the potential energy difference of neutrons and protons on the vector and axial response of the nuclear medium. While the work [20] includes some impacts of the potential difference, it also neglects some aspects: 1) It does not include the impact of the potential difference on the hadronic part of the weak interaction matrix element. At high densities and/or large neutrino energies, these missing terms may impact neutrino charged current mean free paths. 2) It assumes that the nucleon weak charged vector current is conserved, but is not the case because of differences between neutron and proton masses and their dispersion relations in dense matter [28]. This will result in a different structure for the charged current mean field polarization

*Electronic address: robertsl@nscl.msu.edu
†Electronic address: sareddy@uw.edu

tensor. The correct inclusion of these extra terms is likely to impact the response of the medium when correlations are included through the RPA (see below). 3) They neglected weak magnetism corrections, which can be important for predicting the difference between electron neutrino and electron anti-neutrino spectra and nucleosynthesis in the neutrino driven wind, as well as the deleptonization rates of protoneutron stars [29].

As a base line for future studies that would include correlations, we derive for the first time the charged current absorption rates for electron neutrinos which include all of the following effects: 1) different mean-field potential energy shifts for neutrons and protons in neutron-rich matter; 2) relativistic contributions to the nucleon charged currents; 3) weak magnetism; and 4) effects due to the violation of the isospin symmetry, and consequently the lack of conservation of the nucleon charged current in asymmetric matter [28]. We provide derivations of these results both from the perspective of Fermi's Golden Rule, and in the language of finite temperature quantum field theory. In the neutral current limit, these expressions reduce to those given in [22] (up to a sign in one part of the tensor-tensor polarization function). A library for calculating neutrino interaction rates based on this work is available at https://bitbucket.org/lroberts/nuopac.

The paper is structured as follows: In section II, we derive the general form of the charged current opacity from Fermi's Golden Rule. In section II A, we calculate the full charged current polarization tensor and show that its imaginary part agrees with the Fermi's Golden Rule results. We then present practical representations of the response in section II B. We also discuss some approximations to the charged current absorption rate in section II C. In section III, we present limiting forms of the rates and assess the impact of the new terms. Throughout, we set $\hbar = c = k_B = 1$ and use a metric with signature $(+---)$.

II. CHARGED CURRENT OPACITY

The charged current interaction at low energies is described by the Fermi weak interaction Lagrangian

$$\mathcal{L} = \frac{CG_F}{\sqrt{2}}\; l_\mu\; j^\mu_{\rm cc}\,, \tag{1}$$

where $l_\mu = \bar{l}\gamma_\mu(1-\gamma_5)\nu$ is the lepton charged current, $C = \cos\theta_c$ is the cosine of the Cabibbo angle, and

$$j^\mu_{\rm cc} = \bar{\Psi}_p\; \left(\gamma^\mu(g_V - g_A\gamma_5) + F_2\frac{i\sigma^{\mu\alpha}q_\alpha}{2M}\right)\; \Psi_n \tag{2}$$

is the nucleon charged current which includes the vector, axial vector, and weak magnetism contributions, characterized by coupling strengths $g_V = 1$, $g_A = 1.26$, and $F_2 = 3.71$, respectively, and $M = (M_n + M_p)/2 = 938.9$ MeV and M_p, M_n are the proton and neutron masses, respectively. Here, the currents are written using Dirac spinors Ψ_i, l and ν and the γ matrices are in the Dirac basis with $\gamma_5 = i\gamma^0\gamma^1\gamma^2\gamma^3$ and $\sigma^{\mu\nu} = i(\gamma^\mu\gamma^\nu - \gamma^\nu\gamma^\mu)/2$. The cross-section for the two-particle process, $l_1 + N_2 \rightarrow l_3 + N_4$, where l_1 and l_3 are the initial and final state leptons, and N_2 and N_4 are the initial and final state nucleons, respectively, can be calculated from Fermi's Golden Rule. In the relativistic formalism, the differential cross-section for the process $1+2\rightarrow 3+4$ is given by

$$d\sigma = \frac{1}{(2E_1)(2E_2^*)\;v_{\rm rel}}\;\left\langle|M|^2\right\rangle\;d\Phi_{34}(2\pi)^4\delta^4(p_1^\mu + p_2^\mu - p_3^\mu - p_4^\mu)\,, \tag{3}$$

where $v_{\rm rel}$ is the relative velocity between particles in the initial state,

$$d\Phi_{34} = \frac{d^3p_3}{(2\pi)^3 2E_3}\frac{d^3p_4}{(2\pi)^3 2E_4^*}(1-f_3)(1-f_4)\,, \tag{4}$$

is the Lorentz invariant phase which includes effects due to Pauli blocking of the final states and $\langle|M|^2\rangle$ is the square of the matrix element – averaged over initial spin states and summed over the final spin states. Above, $E_i^* = \sqrt{p_i^2 + (M_i^*)^2}$ and M_i^* are the nucleon effective masses in the medium. The differential absorption rate for a neutrino with energy E_1 in the medium where the density of the particle 2 is n_2 is given by

$$d\Gamma(E_1) = \langle n_2\; v_{\rm rel}\; d\sigma\rangle = 2\int\frac{d^3p_2}{(2\pi)^3}\;f_2\;v_{\rm rel}\;d\sigma\,, \tag{5}$$

where f_2 is the distribution of the particle 2 in the medium and the factor of 2 on the RHS accounts for its spin degeneracy. The distribution functions f_i are assumed to be Fermi-Dirac distributions characterized by chemical

potential μ_i and temperature T. Using the standard decomposition of the square of weak matrix element for free nucleons in terms of the lepton tensor and the baryon tensor, we find that

$$\left\langle |M|^2 \right\rangle = \frac{C^2 G_F^2}{4} L_{\mu\nu} \Lambda^{\mu\nu} \,. \tag{6}$$

The lepton tensor is

$$L^{\mu\nu} = \mathrm{Tr}\left[(-\not{p}_1 + m_1)\gamma^\mu(1-\gamma^5)(-\not{p}_3 + m_3)\gamma^\nu(1-\gamma^5)\right] \,, \tag{7}$$

where $q^\mu = p_1^\mu - p_3^\mu = p_4^\mu - p_2^\mu$ is the energy-momentum transfer from the leptons to the baryons. In our case since particle 1 is a neutrino $m_1 \approx 0$ and $m_3 = m_l$ where m_l is the final charged lepton, $m_l = m_e$ for electrons and $m_l = m_\mu$ muons, in the final state. The upper sign is for neutrinos while the lower sign is for antineutrinos, due to their left and right handed character. We use the standard Feynman slash notation, where a slash denotes contraction of a four-vector with the gamma matrices.

Inspecting the kinematics of the leptons gives the allowed range of values for the energy and momentum transfer to the nucleons for given four-momentum of particle 1,

$$q = \sqrt{p_1^2 + p_3^2 - 2p_1 p_3 \mu_{13}} \tag{8}$$

$$q_0 = E_1 - E_3 \,, \tag{9}$$

where μ_{13} is the cosine of the angle between the momentum vectors of particles one and three and p_i is the magnitude of the momentum of particle i. The maximum and minimum values of this expression shows that the allowed range of momentum transfers to be $|p_1 - p_3| < q < p_1 + p_3$. When both particles one and three are massless, these relations imply $q_\mu^2 < 0$ and $|q_0| < q < 2E_1 - q_0$, but these constraints do not hold for charged current reactions in which the final state lepton mass cannot be neglected.

The hadronic part of the matrix element is well known in the case of free nucleons, and including mean field corrections in the nucleon spinors only slightly alters its structure. The necessary modifications to the spin-sums are described in Appendix B. Then, the baryon contribution to the matrix element in the mean field approximation is given by

$$\Lambda^{\mu\nu} = \mathrm{Tr}\left[(-\not{\tilde{p}}_2 + M_2^*)\left\{g_V\gamma^\mu - g_A\gamma^\mu\gamma^5 + F_2\frac{i\sigma^{\mu\alpha}\tilde{q}_\alpha}{2M_p}\right\}(-\not{\tilde{p}}_4 + M_4^*)\left\{g_V\gamma^\nu - g_A\gamma^\nu\gamma^5 - F_2\frac{i\sigma^{\nu\alpha}\tilde{q}_\alpha}{2M_p}\right\}\right]. \tag{10}$$

Here $\tilde{p}_2^\mu = (E_2^*, \vec{p}_2)$, $\tilde{p}_4^\mu = (E_4^*, \vec{p}_4)$, and $\tilde{q}^\mu = \tilde{p}_4^\mu - \tilde{p}_2^\mu$. In the presence of background mean fields, the nucleon energies $E_2 = E_k^* + U_2$ and $E_4 = E_{k+q}^* + U_4$, where U_2 and U_4 are mean field potentials for 2 and 4, respectively. The effective masses of the nucleons 2 and 4 in the medium are M_2^* and M_4^*.

We can now recast the absorption rate in Eq. 5 as

$$\frac{d\Gamma(E_1)}{dE_3 d\mu_{13}} = \frac{C^2 G_F^2\, p_3(1 - f_3(E_3))\; L_{\mu\nu}\; \mathcal{I}^{\mu\nu}}{32\pi^2 E_1 (1 - \exp\left(-(q_0 + \Delta\mu)/T\right))} \tag{11}$$

as in [20]. The nuclear part is now factored and contained in the tensor

$$\begin{aligned} \mathcal{I}^{\mu\nu} &= \int \frac{d^3p_2}{(2\pi)^3 2E_2^*} \int \frac{d^3p_4}{(2\pi)^3 2E_4^*} \left(f_2(E_2) - f_4(E_4)\right) \Lambda^{\mu\nu} (2\pi)^4 \delta^3(\vec{p}_2 - \vec{p}_4 - \vec{q}) \delta(E_2 - E_4 - q_0) \\ &= \int \frac{d^3p_2}{(2\pi)^2}\; \Lambda^{\mu\nu}\; \frac{f_2(E_2) - f_4(E_4)}{4E_2^* E_4^*} \delta(E_2 - E_4 - q_0) \,, \end{aligned} \tag{12}$$

where $E_{k+q}^* = \sqrt{(\vec{k} + \vec{q})^2 + (M_4^*)^2}$ and in the second line we have employed the momentum space Dirac delta function. The detailed balance factor for charged current reactions, $(1 - \exp\left(-(q_0 + \Delta\mu)/T\right))^{-1}$, comes from using the relation $f_2(1 - f_4) = (f_2 - f_4)/(1 - \exp[-(E_4 - E_2 - \mu_4 - \mu_2)/T])$.

Eq. 11 together with Eq. 12 can be used to calculate the charged current opacity. This would include corrections due to mean field potentials, relativistic kinematics and weak magnetism. We calculate $\mathcal{I}_{\mu\nu}$ in detail in section II B, but first we show that the same result can be found from linear response theory.

A. The Charged Current Polarization Tensor

The neutrino absorption rate in nuclear matter can be calculated using linear response theory because at leading order in the weak interaction, the nucleonic and leptonic parts factorize. For the weak interaction Lagrangian in Eq. 1 linear response theory predicts [18, 30]

$$\frac{d\Gamma(E_1)}{dE_3 d\mu_{13}} = \frac{C^2 G_F^2}{32\pi^2}\frac{p_3}{E_1}(1-f_3(E_3))L_{\mu\nu}\ \mathcal{S}^{\mu\nu}(q_0,q)\,, \tag{13}$$

where $L_{\mu\nu}$ is the lepton tensor defined earlier in Eq. 7,

$$\mathcal{S}^{\mu\nu}(q_0,q) = \frac{-2\ \mathrm{Im}\ \mathbf{\Pi}^{\mu\nu}(q_0,q)}{1-\exp\left(-(q_0+\Delta\mu)/T\right)}\,, \tag{14}$$

is called the dynamic response function, and

$$\mathbf{\Pi}^{\mu\nu}(q_0,q) = -i\int dt\ d^3x\ \theta(t)\ e^{i(q_0 t-\vec{q}\cdot\vec{x})}\langle\ |[j_\mu\ (\vec{x},t), j_\nu(\vec{0},0)]|\ \rangle\,, \tag{15}$$

is the retarded current-current correlation function or the polarization tensor where j_μ is the weak charged current defined in Eq. 2 and $\langle|\cdots|\rangle$ is the thermodynamic average $= \mathrm{Tr}\ [\exp(\beta(H-\sum_i \mu_i N_i))\cdots]/\mathcal{Z}$ where $\mathcal{Z}$ is the grand canonical partition function. The relationship in Eq. 14 between the correlation function and the dynamic structure factor is often called the *fluctuation-dissipation* theorem [31, 32].

This correlation function encodes all of the complexities associated with interaction between nucleons in the plasma and is in general difficult to calculate. When nucleons are treated as non-interacting particles, the polarization tensor can be calculated using the free single particle Greens functions. We use the imaginary time formalism [33], where the free nucleon propagator at zero chemical potential is given by

$$\mathcal{G}_{\mathcal{F}}(i\omega_n,\mathbf{p}) = \frac{M-\not{p}}{E_p^2-(i\omega_n)^2}\,. \tag{16}$$

where ω_n is a Fermionic Matsubara frequency. The extension to non-zero chemical potential is straightforward and is obtained by the replacement $i\omega_n \to i\omega_n+\mu$ (see [33] equation 5.70). The effects due to a space-time independent background mean field potential can also be similarly included since its contribution to the grand canonical Hamiltonian is proportional to $\int d^3x\bar{\Psi}\gamma^0\Psi$, similar to the chemical potential (see Appendix B). Additionally, the numerator, which comes from a spin sum, should be replaced by the spin sums described in Appendix B. These considerations imply that the propagator for nucleons in the dense medium is obtained by replacement $i\omega_n \to i\omega_n+\nu_i$, where $\nu_i = \mu_i - U_i$, and $-\not{p}+M \to -\not{\tilde{p}}+M^*$ which gives

$$\mathcal{G}_{i,MF}(i\omega_n+\nu,\mathbf{p}) = \frac{M^*-\not{\tilde{p}}}{{E^*_{p,i}}^2-(i\omega_n+\nu_i)^2}, \tag{17}$$

where M^* is the effective mass, $\tilde{p}^\mu = (\pm E^*_{i,p}, -\vec{p})$, and $E^*_{i,p} = \sqrt{p^2+(M^*_i)^2}$. Using these propagators, the imaginary time polarization functions are given by

$\mathbf{\Pi}_{ab}(i\omega_m-\Delta\mu,\vec{q}) =$

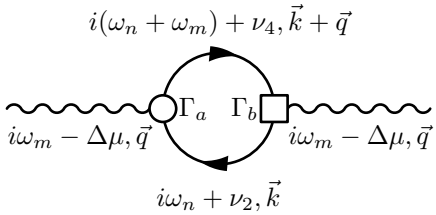

$$= T\sum_n \int \frac{d^3k}{(2\pi)^3}\mathrm{Tr}\left[\mathcal{G}_{2,MF}(i\omega_n+\nu_2,\vec{k})\Gamma_a\mathcal{G}_{4,MF}(i\omega_m+i\omega_n+\nu_4,\vec{k}+\vec{q})\Gamma_b\right], \tag{18}$$

where the Γ_a represent different interaction vertices (i.e. $C_V\gamma^\mu$, etc.), $i\omega_m$ is a Bosonic Matsubara frequency, and $\Delta\mu = \mu_2-\mu_4$.

Using the Matsubara sum results from appendix C and the baryon tensor portion of the weak interaction matrix element given above, we find that the imaginary time polarization tensor is

$$\mathbf{\Pi}_{\mu\nu}(i\omega_m - \Delta\nu, \vec{q}) = \int \frac{d^3k}{(2\pi)^3} \frac{\Lambda_{\mu\nu}}{4E^*_{2,k}E^*_{4,k+q}} \Bigg[\frac{f_2(E^*_{2,k}) - f_4(E^*_{4,k+q})}{i\omega_m - \Delta\nu + E^*_{2,k} - E^*_{4,k+q}} - \frac{\bar{f}_2(E^*_{2,k}) - \bar{f}_4(E^*_{4,k+q})}{i\omega_m - \Delta\nu - E^*_{2,k} + E^*_{4,k+q}} + \frac{1 - f_2(E^*_{2,k}) - \bar{f}_4(E^*_{4,k+q})}{i\omega_m - \Delta\nu + E^*_{2,k} + E^*_{4,k+q}} - \frac{1 - \bar{f}_2(E^*_{2,k}) - f_4(E^*_{4,k+q})}{i\omega_m - \Delta\nu - E^*_{2,k} - E^*_{4,k+q}} \Bigg], \tag{19}$$

where $\Delta\nu = \nu_2 - \nu_4$.

When considering scattering and capture processes, we only require portions of the polarization that are non-zero for $\tilde{q}^2_\alpha < (M^*_2 - M^*_4)^2$ due to kinematic restrictions, so the last two pieces of the polarization can be ignored. The piece of the polarization containing only anti-baryon distribution functions is only non-zero at very high temperatures not encountered in supernovae and neutron star mergers. Therefore, the last three terms in Eq. 19 will be neglected in the rest of the discussion, although we keep in mind the second term will be present when calculating scattering rates from electrons and positrons.

For the linear response, we require the real-time polarization function. This can be found by analytically continuing the imaginary-time polarization [30] via the replacement $i\omega_m - \Delta\mu \to q_0 + i\eta$. The need for this particular replacement can be seen in the incoming and outgoing Bosonic lines in the bubble diagram above, which include a chemical potential difference because the Bosonic frequencies carry isospin charge. Analytically continuing to real-time and using the relation

$$\frac{1}{\omega \pm i\eta} = \mathcal{P}\frac{1}{\omega} \mp i\pi\delta(\omega), \tag{20}$$

we then find the real and imaginary parts of the polarization tensor are given by

$$\mathrm{Im}\mathbf{\Pi}^R_{\mu\nu}(q_0, q) = -\pi \int \frac{d^3k\,\Lambda_{\mu\nu}}{(2\pi)^3 4E^*_{2,k}E^*_{4,k+q}} \delta(E^*_{2,k} - E^*_{4,k+q} + \tilde{q}_0)\{f_2(E^*_{2,k}) - f_4(E^*_{4,k+q})\} \tag{21}$$

$$\mathrm{Re}\mathbf{\Pi}^R_{\mu\nu}(q_0, q) = \mathcal{P} \int \frac{d^3k\,\Lambda_{\mu\nu}}{(2\pi)^3 4E^*_{2,k}E^*_{4,k+q}} \frac{f_2(E^*_{2,k}) - f_4(E^*_{4,k+q})}{E^*_{2,k} + \tilde{q}_0 - E^*_{4,k+q}}, \tag{22}$$

where $\tilde{q}_0 = q_0 + U_2 - U_4$. Note that we are not taking the imaginary part of Λ in this expression.

From this, it is clear that the mean field polarization function is just the free fermion polarization function with the replacements

$$\mu_i \to \nu_i \tag{23}$$

$$q^\mu \to \tilde{q}^\mu = (q_0 + U_2 - U_4, -\vec{q}), \tag{24}$$

where $\tilde{q}^\mu$ is the kinetic energy and momentum transfer from the entrance channel nucleon to the final state nucleon. Comparing Eq. 11 and Eq. 13 we see that linear response theory and the Fermi's Golden Rule approach would yield the same result when

$$\mathcal{I}^{\mu\nu}(q_0, q) = (1 - \exp\left(-(q_0 + \Delta\mu)/T\right))\mathcal{S}^{\mu\nu}(q_0, q)\,. \tag{25}$$

Neglecting anti-particle and pair contributions in Eq. 21, we can verify the above equation to prove that these approaches are equivalent when correlations are neglected. As we will find, projecting $\mathcal{I}_{\mu\nu}$ along and orthogonal to $\tilde{q}^\mu$ results in simple expressions for the polarizations analogous to the results found in the literature for the case of neutral current polarization tensors.

The advantage of the linear response formalism is that it can be extended to included higher order corrections to the medium response, which cannot be done systematically using the Fermi's Golden Rule approach. For instance, the approach above neglects effects due to screening of the weak interaction by particle-hole pairs in the medium and collective excitations such as the giant isovector dipole resonance and the Gammow-Teller resonance, both of which arise due to strong interactions between nucleons. To include these effects consistently with the mean field ground state of the nuclear medium, the response should be calculated in the Random Phase Approximation (RPA) as discussed earlier in [20]. The response functions in RPA can be formulated using the real and imaginary parts of the polarization tensors derived here.

B. Practical Expressions for $\mathcal{I}^{\mu\nu}$ and $L^{\mu\nu}$

The results described in preceding sections provide formulae to calculate the charged current absorption rates, including weak magnetism and mean field contributions, but their forms are not amenable for use in numerical simulations. Here, we derive simple expressions for the components of the differential absorption rate that can easily be implemented for practical calculations.

1. *Expressions for $\mathcal{I}^{\mu\nu}$*

First we consider the general for of the integrals given in equation 12. We employ the energy space delta function in Eq. 12 to remove the integrals over the nucleon angle and leave a single integral over energy. Transforming the energy space delta function to a delta function in the cosine of the angle between nucleons and enforcing momentum conservation (with the momentum transfered assumed to be in the z-direction), we can write structure function as

$$\mathcal{I}^{\mu\nu} = \frac{1}{(4\pi)^2 q}\int_{M_2^*}^{\infty} dE_2 \int d\Omega_2 \delta(\mu-\mu_0)\theta(E_2-e_m)(f_2-f_4)\Lambda^{\mu\nu}, \tag{26}$$

with $\mu_0 = (\tilde{q}_\mu^2 + 2E_2^*\tilde{q}_0 + M_2^{*2} - M_4^{*2})/2p_2q$. Here, $\beta = 1 + (M_{*,2}^2 - M_{*,4}^2)/\tilde{q}_\mu^2$ and

$$e_m = -\beta\frac{\tilde{q}_0}{2} + \frac{q}{2}\sqrt{\beta^2 - \frac{4M_2^{*2}}{\tilde{q}_\mu^2}}. \tag{27}$$

The physical meaning of this lower limit becomes clearer when it is expressed in terms of [28]

$$\sigma_\pm = 1 - (M_2^* \pm M_4^*)^2/\tilde{q}_\alpha^2. \tag{28}$$

The result is

$$e_m = -\beta\frac{\tilde{q}_0}{2} + \frac{q}{2}\sqrt{\sigma_+\sigma_-}. \tag{29}$$

The allowed range of $\tilde{q}_\alpha^2$ is then given by the range of values for which $\sigma_+\sigma_- \geq 0$, which correspond to $\tilde{q}_\alpha^2 < (M_2^* - M_4^*)^2$ or $\tilde{q}_\alpha^2 > (M_2^* + M_4^*)^2$. Clearly, the first condition enforces the impact of the mass difference in capture processes while the second condition is the appropriate kinematic condition for pair production.

The only terms in the integrated baryon tensor $\mathcal{I}^{\mu\nu}$ that cannot be pulled outside of the integral are power of p_2^μ, since $p_4^\mu = p_2^\mu + \tilde{q}^\mu$. Therefore, $\mathcal{I}^{\mu\nu}$ can be expressed in terms of the tensors

$$I^{\{a_k\}} = \frac{8}{(4\pi)^2 q}\int_{e_m}^{\infty} dE_2 \int d\Omega_2 \Theta(\mu-\mu_0)(f_2-f_4)\tilde{p}_2^{a_1}...\tilde{p}_2^{a_k}. \tag{30}$$

We include the extra factor of 8 for convenience, since $\mathrm{Tr}[\Lambda^{\mu\nu}]$ contains a factor of 8.

Since the nucleons are on-shell, it is easy to show that

$$\tilde{q}_\mu I^{\mu\{a_k\}} = -\frac{\beta\tilde{q}_\mu^2}{2} I^{\{a_k\}}. \tag{31}$$

This relation comes in handy when trying to simplify the different parts of the polarization; when $\Lambda^{\mu\nu}$ contains $(p_2\cdot q)$, it can be replaced with $-\beta q_\mu^2/2$.

The expression for $I^{\mu\nu}$ simplifies if decompose it relative to $\tilde{q}^\mu$. The set of projection tensors that describe this decomposition are shown in Appendix A. This results in the expansion

$$I_{\mu\nu} = \beta^2 I_Q P_{\mu\nu}^Q + I_L P_{\mu\nu}^L + I_T P_{\mu\nu}^{T+} + \beta I_M P_{\mu\nu}^{M+}, \tag{32}$$

where we have pulled out factors of β for convenience. The explicit form of these expansion terms are

$$I_Q = \frac{\tilde{q}_\mu^2}{4\pi q}\int_{e_m}^{\infty} dE_2^*(f_2 - f_4) \tag{33}$$

$$I_L = -\frac{\tilde{q}_\mu^2}{4\pi q^3}\int_{e_m}^{\infty} dE_2^*(f_2 - f_4)(2E_2^* + \beta\tilde{q}_0)^2 \tag{34}$$

$$I_M = -\frac{\tilde{q}_\mu^2}{4\pi q^2}\int_{e_m}^{\infty} dE_2^*(f_2 - f_4)(2E_2^* + \beta\tilde{q}_0) \tag{35}$$

$$I_T = -\frac{1}{2}I_L + \left(\frac{2m_2^2}{\tilde{q}_\alpha^2} - \frac{\beta^2}{2}\right) I_Q. \tag{36}$$

Using Eq. 31, we then find for the lower rank tensors

$$I^\nu = -\frac{2\tilde{q}^\nu\beta}{\tilde{q}_\alpha^2} I_Q - \frac{2n^\nu}{\tilde{q}_\alpha^2} I_M \tag{37}$$

$$I = \frac{4}{\tilde{q}_\alpha^2} I_Q. \tag{38}$$

We are now left with one dimensional integrals over E_2 that can be expressed in terms of ultra-relativistic Fermi integrals. We then find the basic pieces of $\mathcal{I}^{\mu\nu}$ are given by

$$I_Q = \frac{\tilde{q}_\mu^2 T}{4\pi q}\Gamma_0 \tag{39}$$

$$I_L = -\frac{\tilde{q}_\mu^2 T^3}{4\pi q^3}\left[a^2\Gamma_0 + 4a\Gamma_1 + 4\Gamma_2\right] \tag{40}$$

$$I_M = -\frac{\tilde{q}_\mu^2 T^2}{4\pi q^2}\left[a\Gamma_0 + 2\Gamma_1\right] \tag{41}$$

$$I_T = -\frac{1}{2}I_L + \left(\frac{2M_{*,2}^2}{\tilde{q}_\alpha^2} - \frac{\beta^2}{2}\right) I_Q \tag{42}$$

where

$$a = (\beta\tilde{q}_0/T + 2e_m/T) \tag{43}$$

$$\delta_1 = (\mu_2 - U_2 - e_m)/T \tag{44}$$

$$\delta_2 = (\mu_4 - U_4 - \tilde{q}_0 - e_m)/T. \tag{45}$$

with

$$\Gamma_n(\delta_2, \delta_4) = \int_0^\infty dx\ x^n\ \left(f_{\rm FD}(x - \delta_2) - f_{\rm FD}(x - \delta_4)\right)\ , \tag{46}$$

where $f_{FD}(x) = 1/[\exp(x) + 1]$. The function $\Gamma_0 = \ln[(\exp\delta_2 + 1)/(\exp\delta_4 + 1)]$ has a simple analytic form, while the other Γ_n are related to polylogarithmic functions and can either be tabulated or calculated using the highly accurate approximations given in [34].

All that is left to do is evaluate the trace in $\Lambda_{\mu\nu}$ and then decompose the resulting imaginary part of the real-time polarization tensor using the tensors described in Appendix A. We choose to split the baryon tensor into coefficients of the various combinations of weak coupling constants, which defines the quantities

$$\mathcal{I}_{\mu\nu} = g_V^2 I_{\mu\nu}^V + g_A^2 I_{\mu\nu}^A + F_2^2 I_{\mu\nu}^T + g_V g_A I_{\mu\nu}^{VA} + g_V F_2 I_{\mu\nu}^{VT} + g_A F_2 I_{\mu\nu}^{AT}. \tag{47}$$

Each of these coefficient tensors are then decomposed in the form

$$I^{i,\mu\nu} = I_Q^i P_Q^{\mu\nu} + I_L^i P_L^{\mu\nu} + I_{T+}^i P_{T+}^{\mu\nu} + I_{T-}^i P_{T-}^{\mu\nu} + I_{M+}^i P_{M+}^{\mu\nu} + I_{M-}^i P_{M-}^{\mu\nu}, \tag{48}$$

where i denotes either the vector, axial, tensor or mixed portions of the weak interaction.

Calculating the trace of $\Lambda_{\mu\nu}$ is straightforward (we employ the Mathematica package [35]). Using $\Lambda_{\mu\nu}$ in equation 21, we find the non-zero components of the vector polarization are

$$\begin{aligned} I_Q^V &= \left(\lambda^2 + \sigma_- - 1\right) I_Q && (49)\\ I_L^V &= I_L + \sigma_- I_Q && (50)\\ I_{T+}^V &= I_T + \sigma_- I_Q && (51)\\ I_{M+}^V &= I_M \lambda. && (52) \end{aligned}$$

Here, we have defined $\lambda = \beta - 1$ and $\Delta = (M_4^* - M_2^*)/M_2^*$.

The non-zero pieces of the axial polarization are

$$\begin{aligned} I_Q^A &= \left(\lambda^2 + \sigma_+ - 1\right) I_Q && (53)\\ I_L^A &= I_L + \sigma_+ I_Q && (54)\\ I_{T+}^A &= I_T + \sigma_+ I_Q && (55)\\ I_{M+}^A &= I_M \lambda. && (56) \end{aligned}$$

The non-zero pieces of the tensor polarization are

$$\begin{aligned} I_L^T &= \frac{q_\alpha^2}{4m_2^2}\left[\left(\sigma_- - \beta^2 + \frac{4m_2^2}{q_\alpha^2}\right) I_Q - I_L\right] && (57)\\ I_{T+}^T &= \frac{q_\alpha^2}{4m_2^2}\left[\left(\sigma_- - \beta^2 + \frac{4m_2^2}{q_\alpha^2}\right) I_Q - I_T\right]. && (58) \end{aligned}$$

The mixed vector-tensor polarization is

$$\begin{aligned} I_L^{VT} &= (2 + \Delta\beta) I_Q && (59)\\ I_{T+}^{VT} &= (2 + \Delta\beta) I_Q && (60)\\ I_{M+}^{VT} &= -\frac{\Delta}{2} I_M. && (61) \end{aligned}$$

The vector axial piece is

$$I_{T-}^{VA} = -i2 I_M. \quad (62)$$

And finally the axial tensor piece is

$$I_{T-}^{AT} = -i(2 + \Delta) I_M. \quad (63)$$

These expressions are similar to those found in [10, 22], but they include extra terms depending on the mass and potential differences of the nucleons. A detailed comparison between these results and previous results is made in section III B.

2. *The Lepton Tensor*

The contraction of the lepton tensor with the imaginary part of the polarization is the last piece required to calculate the differential neutrino cross-section. The easiest way to perform this contraction is to project the lepton tensor using the same projectors we used for the polarization tensor. Performing these projections gives

$$\begin{aligned} L_L &= \tfrac{8}{\tilde{q}_\alpha^2}\big[\ -2(\tilde{n}\cdot p_1)^2 + 2(\tilde{n}\cdot p_1)(\tilde{n}\cdot q) + \tilde{q}_\alpha^2 (p_1\cdot q)\big]\\ L_Q &= \tfrac{8}{\tilde{q}_\alpha^2}\big[\ 2(\tilde{q}\cdot p_1)^2 - 2(\tilde{q}\cdot p_1)(q\cdot\tilde{q}) + \tilde{q}_\alpha^2 (p_1\cdot q)\big]\\ L_{M+} &= \tfrac{8}{\tilde{q}_\alpha^2}\big[\ (\tilde{q}\cdot p_1)(\tilde{n}\cdot q) + (\tilde{n}\cdot p_1)(q\cdot\tilde{q} - 2\tilde{q}\cdot p_1)\big]\\ L_{M-} &= \tfrac{8i}{\tilde{q}_\alpha^2}\ \ \epsilon^{\alpha\beta\gamma\delta}\tilde{n}_\alpha p_{1,\beta}\tilde{q}_\gamma q_\delta\\ L_{T+} &= \tfrac{8}{\tilde{q}_\alpha^2}\big[\ (\tilde{n}\cdot p_1)^2 - (\tilde{n}\cdot p_1)(n\cdot q) + (\tilde{q}\cdot p_1)(\tilde{q}\cdot q - p_1\cdot\tilde{q})\big]\\ L_{T-} &= \tfrac{8i}{\tilde{q}_\alpha^2}\big[\ (\tilde{n}\cdot p_1)(\tilde{q}\cdot q) - (\tilde{n}\cdot q)(p_1\cdot\tilde{q})\big]. \end{aligned} \quad (64)$$

The contractions appearing above are

$$\begin{aligned} p_1\cdot q &= \frac{q_\alpha^2-m_3^2}{2} \\ p_1\cdot\tilde{q} &= p_1\cdot q+\Delta U E_1 \\ p_1\cdot\tilde{n} &= -\frac{q_\alpha^2}{2q}[E_1+E_3-\Delta U+2\Delta U E_1 q_0/q_\alpha^2+(q_0-\Delta U)m_3^2/q_\alpha^2] \\ \tilde{n}\cdot q &= -q\Delta U \\ q\cdot\tilde{q} &= q_\alpha^2+q_0\Delta U. \end{aligned} \tag{65}$$

In general, the projections of the lepton tensor have relatively complicated forms since we are projecting the lepton tensor relative to $\tilde{q}_\mu$ rather than the more natural q_μ. In the free gas limit and neglecting m_3, these expressions reduce to

$$L_T = 8q_\alpha^2\,(A+1) \tag{66}$$
$$L_L = -8q_\alpha^2 A \tag{67}$$
$$L_Q = 0 \tag{68}$$
$$L_{M+} = 0 \tag{69}$$
$$L_{T-} = \pm i16(n\cdot p_1), \tag{70}$$

where

$$A=\frac{4E_1E_3+q_\alpha^2}{2q^2}=\frac{E_1E_3}{q^2}(1+\mu_{13}), \tag{71}$$

which agrees with expressions previously found in the literature [10, 22].

With these results, the contraction of the lepton tensor and the polarization tensor is quite simple (using the result of Appendix A)

$$L^{\mu\nu}\mathcal{I}_{\mu\nu}=\sum_{i=\{V,A,T,VA,VT,AT\}}\mathcal{C}_i\left[L_L I_L^i+L_Q I_Q^i-2L_{M+}I_{M+}^i-2L_{M-}I_{M-}^i+2L_{T+}I_{T+}^i+2L_{T-}I_{T-}^i\right], \tag{72}$$

where $\mathcal{C}_i=\{g_V^2,g_A^2,F_2^2,g_Ag_V,\ldots\}$ and the differential neutrino cross section can be found using equations 11 and 47.

C. Opacities from a Limiting Form of the Matrix Element

Often, it is assumed that the nucleon masses dominate all other energy scales entering the averaged matrix element [13]. In this approximation,

$$\begin{aligned} \langle|\mathcal{M}|^2\rangle &= 16C^2G_F^2\left[(g_V+g_A)^2(p_1\cdot\tilde{p}_2)(p_3\cdot\tilde{p}_4)+(g_V-g_A)^2(\tilde{p}_2\cdot p_3)(p_1\cdot\tilde{p}_4)-(g_V^2-g_A^2)(p_1\cdot p_3)(\tilde{p}_2\cdot\tilde{p}_4)\right] \\ &\approx 16C^2G_F^2E_1E_3M_2^*M_4^*\left[(g_V+g_A)^2+(g_V-g_A)^2-(g_V^2-g_A^2)(1-\mu_{13})\right], \end{aligned} \tag{73}$$

where the second line is to leading order in the nucleon mass [36]. Following a similar set of steps to those for the full matrix element, we find the approximate cross-section is given by

$$\frac{d\Gamma(E_1)}{dE_3d\mu_{13}}\approx\frac{C^2G_F^2}{4\pi^2}\frac{p_3E_3}{1-\exp[-(q_0+\Delta\mu)/T]}\left[g_V^2(1+\mu_{13})+g_A^2(3-\mu_{13})\right]\frac{4M_2^*M_4^*}{\tilde{q}_\alpha^2}I_Q. \tag{74}$$

This is similar in form to the non-relativistic cross-section given in [10, 20], except that non-relativistic kinematics has not been assumed for the integrals over the nucleon momentum or in e_m. When non-relativistic kinematics are enforced at all momenta, an upper limit in the nucleon energy integral is required to enforce momentum conservation which is clearly spurious. This upper limit gives the second logarithmic factor shown in Eq. 48 of [20]. Additionally, the form of e_m is different when it is calculated using non-relativistic kinematics.

A further approximation that is often assumed due to the large mass of the nucleons is $\vec{q}=0$ in the nucleon integrals and $E_{2,4}^*=M_{2,4}^*$ [11, 37]. In this case, the response function of the medium becomes

$$\begin{aligned} I_{q=0} &= 2\pi\delta(E_2-E_4+q_0)\int\frac{d^3p_2}{(2\pi)^3}(f_2-f_4) \\ &\approx \pi\delta(M_2^*+U_2-M_4^*-U_4+q_0)(n_2-n_4). \end{aligned} \tag{75}$$

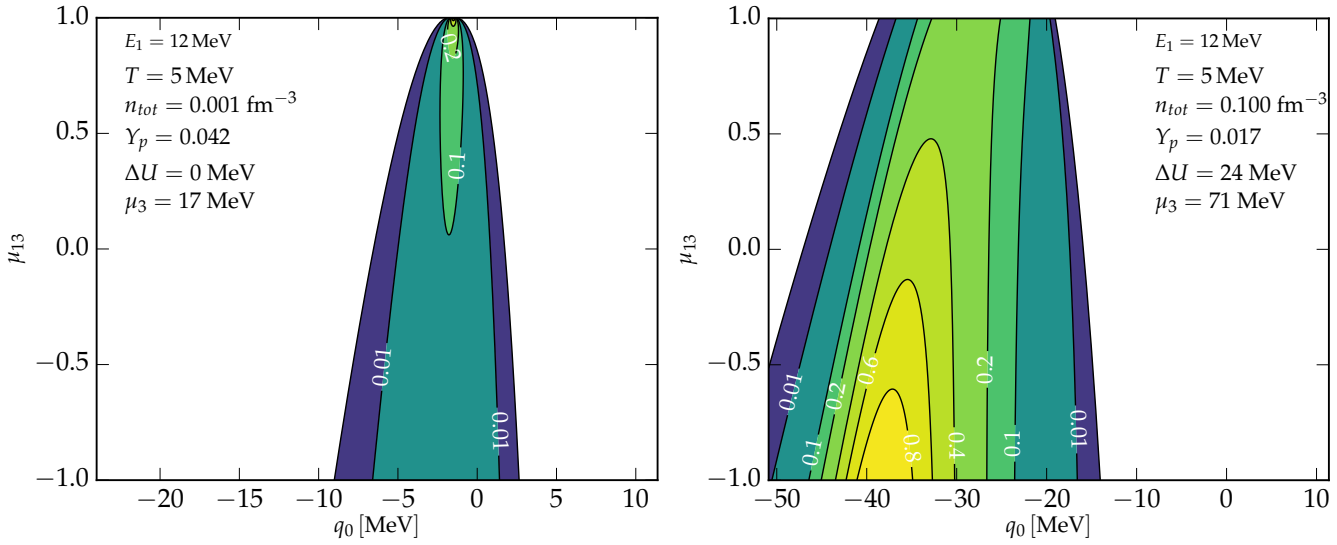

FIG. 1: Contours of the $\nu_e + n \to e^- + p$ double-differential absorption rate as a function of electron scattering angle μ_{13} and energy transfer q_0, normalized to the integrated absorption rate.

The second line follows from assuming $p^2/(2M_2^*) = p^2/(2M_4^*)$. Then, the differential cross section is given by

$$\frac{d\Gamma(E_1)}{dE_3 d\mu_{13}} \approx \frac{C^2 G_F^2}{2\pi^2} \frac{p_3 E_3}{1 - \exp[(\Delta M^* + \Delta U - \Delta\mu)/T]} I_{q=0} \left[g_V^2 (1 + \mu_{13}) + g_A^2 (3 - \mu_{13}) \right], \tag{76}$$

which gives the standard integrated cross section per volume

$$\frac{\sigma}{V} = \frac{C^2 G_F^2}{\pi} (g_V^2 + 3g_A^2) p_3 E_3 \frac{n_2 - n_4}{1 - \exp[(\Delta M^* + \Delta U - \Delta\mu)/T]}. \tag{77}$$

These approximate forms of the cross section will be compared to the full results below.

III. RESULTS

Here, we present differential cross sections and comparison to previous results in the literature. In the charged current rates, the potential energy difference between neutrons and protons can play a dominant role in the capture mean free paths of neutrinos in the medium. This potential difference depends on the effective nuclear interaction that is assumed and is therefore model dependent. For illustrative purposes in this section, we choose a very simple density dependent potential energy given by

$$\Delta U = \Delta U_0 \frac{(n_2 - n_4)}{n_{\rm sat}}, \tag{78}$$

where $n_{\rm sat} = 0.16$ fm^{-3} and we choose a coupling value of $\Delta U_0 = 40$ MeV and keep the nucleon masses fixed at their vacuum values for all densities. At very low and high densities, a linear model for the potential energy is unrealistic. Therefore, we emphasize that the results using this model for the potential are only for illustrative purposes. We choose this model only for its simplicity and because it prevents us from having to choose from the plethora of relativistic mean field theories available. Additionally, we keep the nucleon masses fixed to their vacuum values for most of the discussion for simplicity, although we consider the impact of varying the effective nucleon mass at saturation density in section III C. It is important to note that the formalism presented above fully accounts for the impact of effective nucleon masses on the neutrino absorption rate and the publicly available code associated with this paper can be used to assess the impact of any variation in the nucleon effective masses.

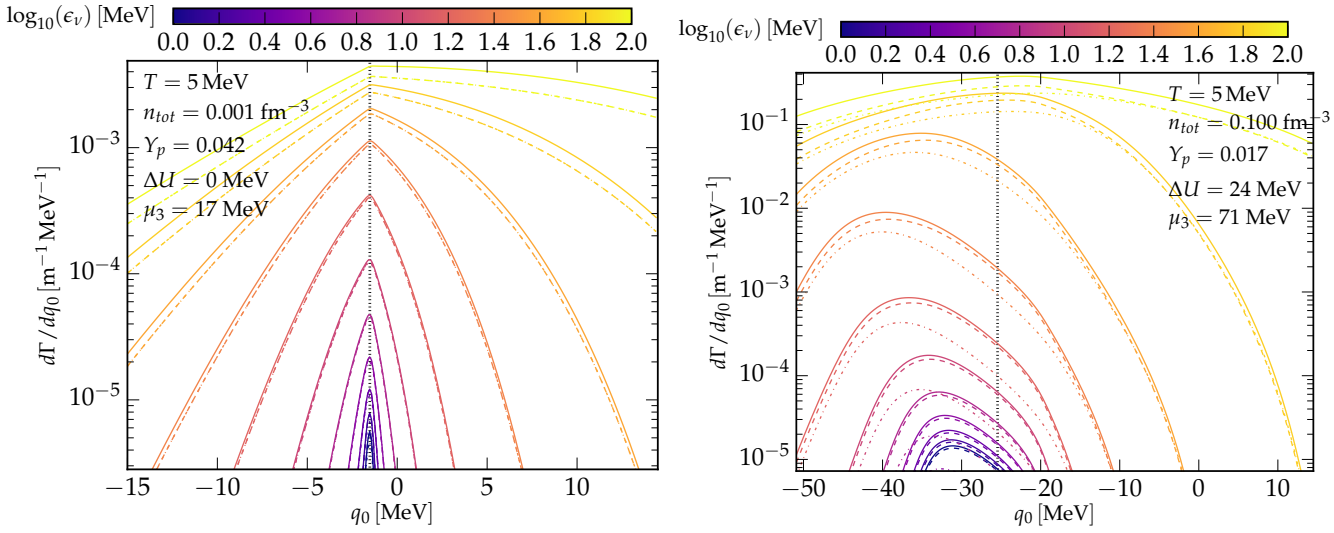

FIG. 2: The angle integrated cross section as a function of energy transfer q_0 for $\nu_e + n \to e^- + p$. The right panels show $\nu_e + n \to e^- + p$ while the right panels show the reaction $\nu_e + n \to \nu_e' + n$. The dotted black lines shows the position of the energy transfer peak when final state blocking is not included, $U_4 - U_2 + M_4^* - M_2^*$. The solid lines show our full expressions for the cross section, the dot dashed lines show the full expressions neglecting tensor corrections, and the dashed lines show the [10] prescription for the cross section.

A. Differential Cross Sections

The main results of this work are differential charged current neutrino cross-sections. In general, the electron scattering angle and energy transfer are integrated over to give the mean free paths which are relevant to transport calculations. Nevertheless, to give the reader a feeling for the structure of these results, we show here some representative differential cross sections.

First, we consider the structure of the full double differential absorption. In figure 1, we show the this quantity at low density and at high density. It is strongly peaked at the q_0 expected for small momentum transfer. The variation with scattering angle is given by the leading order $1/q = 1/\sqrt{E_1 + E_3 - 2E_1E_3\mu_{13}}$ dependence of the baryon response combined with the lepton kinematics. Based on the elastic limit of the cross section we expect a weak angular dependence in the lepton kinematics of the form $1 + (C_V^2 - C_A^2)/(4C_V^2 + 12C_A^2)\mu_{13} \approx 1 - 0.11\mu_{13}$. The combination of these two factors gives the strongly forward peaked differential cross section with a more slowly varying backward scattering tail. This leading order behavior only holds for neutrinos with energies small compared to the baryon mass. At high density these limiting expressions for the scattering angle dependence also break down and the structure of the differential cross section is altered. For the conditions shown in the right panel of 1, it is slightly backward peaked and has strength at a much larger range of energy transfers.

Second, we consider the angle integrated differential cross section $d\sigma/dq_0$, which encodes the energy transfer between the leptons and baryons. For charged current reactions, we expect this quantity to be peaked at $U_4 - U_2 + M_4^* - M_2^*$ when electron final state blocking is ignored, since this is the most favorable energy for small momentum transfer [11, 13]. In figure 2, this cross section is shown. The left panel shows the charged current differential cross-section at low density. Here, the electrons are not strongly degenerate and the peak of the differential cross section is at the zero momentum transfer value for all but the smallest neutrino energies shown. In contrast, at the high density shown in the right panel, the differential cross section peaks away from the zero momentum transfer value because the term $1 - f_3(E_3)$ depends exponentially on q_0. Therefore, there is significantly stronger dependence on the value of the differential cross section away from the zero momentum transfer peak, which is often more poorly captured in approximations to the charged current rates.

We can also start to see how the various corrections included in the rates derived above alter the differential cross section. There, the tensor corrections impact the normalization of the cross-section significantly, increasing to a correction of $\sim 25\%$ for the highest energy neutrinos, but they do not impact the energy transfer. At high density, where ΔU is larger and electron final state blocking can be significant, the variation between different approximations to the charged current rates can be large. It is also clear that the expressions of [10] differ significantly from those derived here. We consider these differences in detail in the next section.

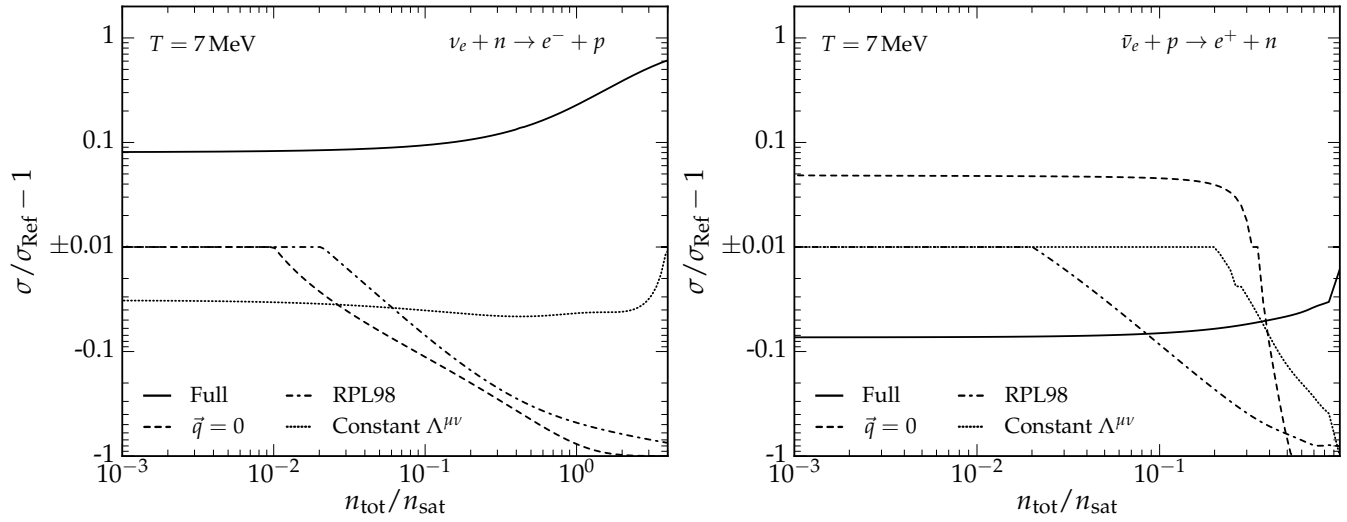

FIG. 3: Comparison of various approximations to the charged current cross section per nucleon as a function of density in beta-equilibrated matter. The reference cross section, σ_{Ref} is taken to be the full cross section without weak magnetism corrections (i.e. $F_2 = 0.0$). The neutrino energy is assumed to be πT. The left panel shows the reaction $\nu_e + n \to e^- + p$ while the right panel shows $\bar{\nu}_e + p \to e^+ + n$. The electron antineutrino cross sections are only shown up to threshold. Full denotes the fully relativistic cross section including weak magnetism corrections, $\vec{q} = 0$ is the cross section given by Eq. 76, RPL98 denotes the cross section given by the expressions in [10], and Constant $\Lambda^{\mu\nu}$ refers to the cross section given by Eq. 74.

B. Comparison with earlier work

We now turn to compare our results for the charged current cross sections in neutron-rich nuclear matter including weak magnetism to a number of other approximations for different ambient conditions. The comparisons are shown in figure 3. We take the full expression with $F_2 = 0.0$ (i.e. the full cross section without weak magnetism corrections) as a baseline for comparison. The simplest approximation to the charged current rates including mean field effects is given by equation 76. At low density, this approximation agrees with the full cross section without weak magnetism at the percent level for $\nu_e + n \to e^- + p$. The deviation is somewhat larger for electron antineutrino capture. Once the density becomes high enough for final state blocking to be important, this approximation starts to strongly deviate from the full expression and drastically under predicts the cross section at saturation density and above for both electron neutrinos and antineutrinos. These conclusions are likely to be impacted when the effective masses have a more complex density dependence.

The second approximation we consider comes from assuming a constant hadronic portion of the matrix element (see Eq. 74). This results in expressions that are very similar to the non-relativistic results given by [10, 19]. At low density, this approximation agrees with our baseline result to a few percent. This is not surprising given that this approximation should be accurate to order q/M. At higher densities, this approximation breaks down for the antineutrino capture rate.

The inclusion of the full weak magnetism correction induces corrections of order 10% for the 22 MeV neutrinos considered in the plot, with the correction going in opposite directions for neutrino and antineutrino capture. Near saturation density, the weak magnetism corrections begin to become significantly larger than would be predicted by the expansion given in [29].

A similar description of the relativistic charged current differential neutrino cross sections was given in [10]. We find the following significant differences from that work:

1. The difference between neutron and proton masses and self-energies was not properly accounted for in the calculation of the polarization tensor. Specifically, the integrals needed to calculate the polarization function defined in eqns. 34, 35, 36, and 36 depend on β and $\tilde{q}_0$. These dependencies were neglected in [10] where $\beta = 1$ and $\tilde{q}_0 = q_0$ was used [1].

[1] This appears to be a typographical error because the code used to generate these results in [10] did account for corrections arising from $\beta \neq 1$ and $\tilde{q}_0 \neq q_0$.

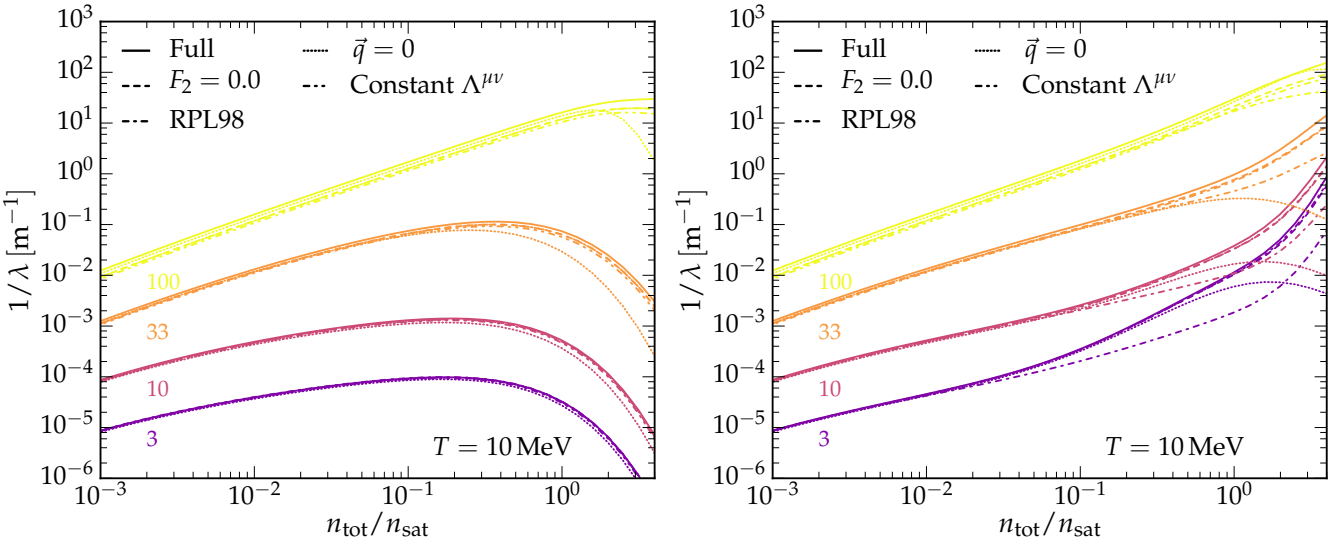

FIG. 4: The $\nu_e + n \to e^- + p$ mean free path as a function of total density for neutrino energies $\{3, 10, 33, 100\}$ MeV. The full cross section (solid lines), the full cross section neglecting weak magnetism (dashed lines), the [10] expression for the cross section (dot-dashed lines), the non-relativistic elastic limit (dotted lines), and the constant $\Lambda_{\mu\nu}$ matrix element limit (dot-dot-dashed lines) of the cross section are all shown. The left panel shows the results for a free gas of protons and neutrons, while the right panel shows the results for a gas with a mean field potential as described in the text. At low density, all of the approximations agree reasonably well (although there are significant deviations for higher energy neutrinos), but at higher density and for finite ΔU they diverge significantly.

2. Current conservation, which requires $q^\mu \Pi^V_{\mu,\nu} = 0$, was used to related different components of the polarization tensor in [10]. Differences between the neutron and proton masses and self-energies violates this relation [28], and contracting the vector piece of the polarization with the mean field corrected energy momentum transfer gives

$$\tilde{q}^\mu I^V_{\mu\nu} = I^V_Q \tilde{q}^\nu + I^V_{M+} \tilde{n}^\nu \neq 0\,, \tag{79}$$

and since $I^V_{\mu\nu} \propto \Pi^V_{\mu\nu}$, $q^\mu \Pi^V_{\mu\nu} \neq 0$ in general. These corrections become significant when $U_2 - U_4$ is large compared to the neutrino energy.

3. There is typographical error in Eq. 69 and 70 of Ref. [10] where the lower limit of the energy integral was defined. The correct expression defined here in Eq. 27 differs by a sign.

4. As discussed in II B 2, the lepton tensor in [10] was calculated by setting the charged lepton mass to zero because it was assumed that their energies would be relatively large. The associated correction for reactions involving electron neutrinos is typically negligible, since $E_e \gg m_e$ but can be important for charged current reactions involving muon neutrinos.

These differences significantly alter the charged current cross sections in regions where the ΔU is significant, as can be seen in figure 3.

In figure 4, the absorption mean free path in beta-equilibrated matter is shown for a range of neutrino energies in all of the approximations described above. In the left panel, we show the mean free path in a non-interacting medium. At low density, all of the different expressions for the capture rate agree reasonably well, with deviations increasing with increasing neutrino energy. At high density, the cross section per nucleon is suppressed due to final state electron blocking. This causes the $\vec{q} = 0$ cross section for higher energy neutrinos to be in error by factors of a few because of its delta function distribution of allowed energy transfer, since the full nucleon response is broadly peaked in q_0 for these neutrinos (see above in section III A). All of the other approximations for the cross section agree at the few tens of percent level across all densities for a non-interacting gas. The inclusion of weak magnetism corrections only has a small impact, with the size of the correction increasing with neutrino energy [22].

When interactions are included, the differences between the various approximations become more substantial, as was described above. Additionally, the inclusion of mean field potentials has a strong impact of the mean free paths relative to the free gas case [11, 13]. This is shown in the right panel of figure 4. At high density and low neutrino

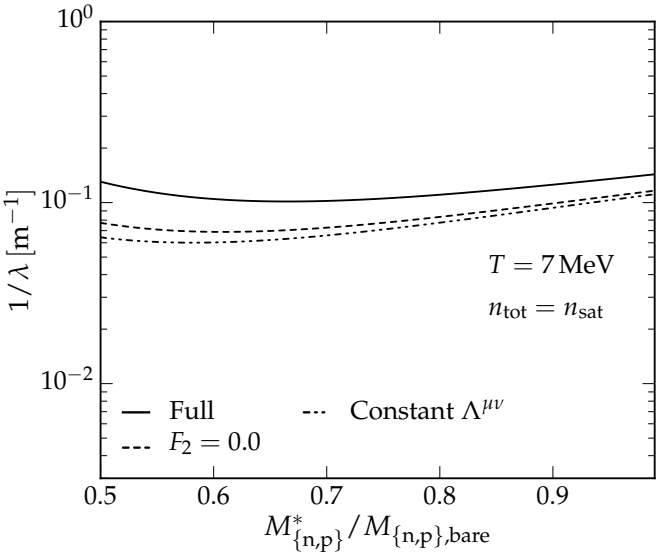

FIG. 5: Variation of the charged current neutrino mean free path with the nucleon effective masses at saturation density. The nucleon effective mass is assumed to be isospin independent and matter is assumed to be in beta-equilibrium. The neutrino energy is taken to be $E_\nu = \pi T$. Full denotes the fully relativistic cross section including weak magnetism corrections, RPL98 denotes the cross section given by the expressions in [10], and Constant $\Lambda^{\mu\nu}$ refers to the cross section given by Eq. 74.

energy, the largest deviations between the results in [10] and our results are seen. The density at which significant deviations begin increases with increasing neutrino energy. For smaller neutrino energies, ΔU becomes the dominant energy scale at lower density than for higher energy neutrinos. Similarly to the non-interacting case, the $\vec{q} = 0$ results strongly under predict the inverse mean free path at high density when final state blocking becomes larger. As we saw above, constant $\Lambda_{\mu\nu}$ approximation agrees with the full expression without weak magnetism quite well, although the deviations between the two get larger with increasing neutrino energy. We expect the differences would also get larger in models where the nucleon effective mass is significantly less than the nucleon rest mass and other energy scales entering the response function become closer to the in-medium nucleon mass. Finally, it can be seen the corrections from the inclusion of weak magnetism are similar to those in the non-interacting case.

C. Nucleon Effective Masses

In the illustrative calculations above, we kept the nucleon masses fixed at their vacuum values for simplicity. In the nuclear medium, nucleon effective masses can be significantly different from their bare values. In non-degenerate matter, we expect the dependence of the mean free path on the isospin independent effective mass to be weak [20]. On the other hand, in degenerate matter the leading order $M_2^* M_4^*$ dependence of the differential cross-section remains after integration over q_0 and μ_{13} [20]. Therefore, we expect that reducing the nucleon effective mass will reduce the neutrino mean free path but at the a rate slower than M^2. In figure 5, we show the impact of varying the nucleon effective masses at saturation density in beta-equilibrium assuming the effective masses are isospin independent. The expected reduction in the mean free path is seen in all approximations of the neutrino mean free path down to $M^*/M \approx 0.6$. Because the chemical potentials in beta-equilibrium depend on the effective mass, $\hat{\mu}$ decreases with increasing effective mass in Figure 5. Therefore, the detailed balance factor gets larger for smaller effective masses and eventually becomes more important than the leading order mass dependence in the response, causing the turnover in the behavior of the mean free path with effective mass seen at the lowest effective masses considered here.

It is also likely that there is significant isospin dependence of the effective mass [38]. The formalism developed here can fully account for this. To leading order, isospin splitting of the effective mass provides a similar effect to isospin dependent potential energies, since the charged current response will be peaked around $q_0 = U_4 - U_2 + M_2^* - M_4^* = 0$. Including this isospin dependence in the effective masses in a manner consistent with constraints on the nuclear symmetry energy requires also choosing different values for the nucleon potential energies. A detailed investigation of the impact of isospin dependent effective masses on neutrino opacities is beyond the scope of this work.

D. The Neutral Current Limit

Since the neutral current interactions have the same mass and potential for the incoming and outgoing baryons, we set $\beta = 1$, $\lambda = \Delta = 0$, $\sigma_- = 1$, $\sigma_+ = 1 - 4m_2^2/q_\alpha^2$, and $\tilde{q}_0 = q_0$. With these replacements, only two pieces of the vector polarization are non-zero

$$\begin{aligned} I_L^{V,nc} &= I_Q + I_L \\ &= -\frac{q_\mu^2}{4\pi q^3}\int_{e_m}^{\infty} dE_2(f_2 - f_4)\left[(2E_2 + q_0)^2 - q^2\right] \qquad (80) \\ I_T^{V,nc} &= I_Q + I_T \\ &= -\frac{q_\mu^2}{4\pi q^3}\int_{e_m}^{\infty} dE_2(f_2 - f_4)\left[q^2/2 + 2M_2^2\frac{q^2}{q_\alpha^2} + (2E_2 + q_0)^2/2\right] \qquad (81) \end{aligned}$$

which has the same form as the results of [10] (although there is a factor of two difference, which is purely definitional). For the neutral current reactions, vector current conservation holds for the polarization tensor, such that $q_\mu I_V^{\mu\nu} = 0$, which can be seen from substituting the neutral current expressions in Eq. 79. Therefore, the standard decomposition of the vector part of the neutral current polarization tensor is

$$I_{\mu\nu}^{V,nc} = I_L^{V,nc} P_{\mu\nu}^L + I_T^{V,nc} P_{\mu\nu}^T, \qquad (82)$$

which gives $I_L^{V,nc} = -\frac{q_\mu^2}{q^2} I_{00}^{V,nc}$ and $I_T^{V,nc} = -I_{22}^{nc}$, which has been used in previous works [10, 14].

We can also see that

$$I_{\mu\nu}^{A,nc} = I_L^{V,nc} P_{\mu\nu}^L + I_T^{V,nc} P_{\mu\nu}^T + \eta_{\mu\nu} I_A \qquad (83)$$

with

$$I_A = -\frac{4M_2^2}{q_\alpha^2} I_Q = -\frac{M_2^2}{\pi q}\int_{e_m}^{\infty} dE_2(f_2 - f_4), \qquad (84)$$

which also agrees with [10]. Our expression for the mixed vector-axial polarization is also in agreement.

The neutral current tensor polarizations were investigated in [22]. Our result is

$$\begin{aligned} I_L^T &= I_Q - \frac{q_\alpha^2}{4m_2^2} I_L = -\frac{q_\alpha^2}{4m_2^2}\left[I_L^V + I_A\left(1 + \frac{q_\alpha^2}{4m_2^2}\right)\right] \qquad (85) \\ I_T^T &= I_Q - \frac{q_\alpha^2}{4m_2^2} I_T = -\frac{q_\alpha^2}{4m_2^2}\left[I_T^V + I_A\left(1 + \frac{q_\alpha^2}{4m_2^2}\right)\right] \qquad (86) \end{aligned}$$

This agrees with [22] up to a sign in front of I_A in I_T^T.

IV. CONCLUSIONS

We have derived complete expressions for charged current neutrino interactions in the mean field approximation, including weak magnetism, arbitrary degeneracy, and relativistic kinematics. We approach the problem both using a Fermi's Golden Rule and the linear response given by many-body perturbation theory to clarify the derivation and provide a path to including correlations. Both approaches of course yield the same answer. We then investigated the neutrino mean free paths predicted by these results and compared them to other results found in the literature. These expressions can also be used to calculate neutral current cross sections and inelastic electron scattering. We provide an open source library for calculating these opacities at https://bitbucket.org/lroberts/nuopac.

Our results extend and correct results previously presented in the literature. We find that vector current non-conservation in charged current reactions [28] and the correct inclusion of neutron and proton potential energies, along with weak magnetism corrections to all orders, introduces a number of new terms in the charged current opacities. At low densities, the corrections to the old rates are modest and provide changes of a few to ten percent relative to previous results in the literature for neutrino energies of order ten MeV. This is unlikely to make qualitative changes in the results of core collapse supernova and compact object merger simulations, but in situations where computational models are sensitive to small changes in microphysics these corrections can at least remove one source of uncertainty.

At high density, especially when the neutron proton self-energy difference is large, they can alter the neutrino mean free paths in the medium by factors of a few or greater. This is likely to impact the rate of lepton transport inside proto-neutron stars.

Additionally, our derivation of the charged current polarization tensor provides a starting point for future calculations of RPA corrections to the charged current rates. Previous work has found that these corrections can change rates by up to factors of a few at and above nuclear saturation density [20, 21]. At sub-nuclear density, more work is warranted to assess the role of particle-hole screening and collective modes. Since the nucleon-nucleon interaction is nearly resonant at low momentum, we are exploring the RPA correlations with large effective interactions that can reproduce nucleon-nucleon phase shifts. This will be reported in a future publication. Additionally, because we find a different tensor structure than was found in previous work [20, 21], the detailed form of the RPA equations will be altered. It remains to be seen if this significantly impacts the resulting opacities. In the future, we also plan to include RPA corrections in our publicly released opacity library.

Acknowledgments

We gratefully acknowledge Ermal Rrapaj for pointing out the chemical potential difference appearing in the Bosonic frequencies of the imaginary time polarization and Vincenzo Cirigliano for many useful discussions. We also thank the participants of the INT workshop INT-16-61W for useful discussions that highlighted the importance of charged current reactions in supernovae.

This research was supported by the NSF under TCAN grant number AST-1333607. S. R. was supported by the US Dept. of Energy Grant No. DE-FG02-00ER41132. This work was enabled in part by the NSF under Grant No. PHY-1430152 (JINA Center for the Evolution of the Elements).

Appendix A: Polarization Tensor Decomposition

Here, we partially follow [33] on pages 113, 118, and 214. First, we choose to decompose the momentum transfer as $\tilde{q}_\mu = (\tilde{q}_0, 0, 0, q)$ and build a second vector orthogonal to $\tilde{q}_\mu$ in the time-z plane, $n_\mu = (q, 0, 0, \tilde{q}_0)$. We then define the transverse projector

$$\begin{aligned} P^{T+}_{\mu\nu} &= \eta_{\mu\nu} - \frac{\tilde{q}_\mu \tilde{q}_\nu}{\tilde{q}^2_\mu} - \frac{n_\mu n_\nu}{n^2} \\ &= \eta_{\mu\nu} + \frac{n_\mu n_\nu - \tilde{q}_\mu \tilde{q}_\nu}{\tilde{q}^2_\mu}, \end{aligned} \tag{A1}$$

which picks out the portion of a vector orthogonal to $\tilde{q}_\mu$ and n_μ. We can also define the projectors along $\tilde{q}_\mu$ and n_μ as

$$P^{L}_{\mu\nu} = \frac{n_\mu n_\nu}{n^2_\mu} = -\frac{n_\mu n_\nu}{\tilde{q}^2_\mu} \tag{A2}$$

$$P^{Q}_{\mu\nu} = \frac{\tilde{q}_\mu \tilde{q}_\nu}{\tilde{q}^2_\mu}. \tag{A3}$$

It is also useful to define the quantities

$$P^{M\pm}_{\mu\nu} = \frac{\tilde{q}_\mu n_\nu \pm \tilde{q}_\nu n_\mu}{\tilde{q}^2_\mu} \tag{A4}$$

$$P^{T-}_{\mu\nu} = \epsilon_{\mu\nu\lambda\delta} \frac{\tilde{q}^\lambda n^\delta}{\tilde{q}^2_\alpha} \tag{A5}$$

The only non-zero, complete contractions of these tensors with one another are

$$P^{L}_{\mu\nu} P^{\mu\nu}_{L} = 1 \tag{A6}$$

$$P^{Q}_{\mu\nu} P^{\mu\nu}_{Q} = 1 \tag{A7}$$

$$P^{M\pm}_{\mu\nu} P^{\mu\nu}_{M\pm} = -2 \tag{A8}$$

$$P^{T\pm}_{\mu\nu} P^{\mu\nu}_{T\pm} = 2. \tag{A9}$$

Any rank two tensor can be decomposed as

$$A_{\mu\nu} = A_Q P^Q_{\mu\nu} + A_L P^L_{\mu\nu} + A_{M+} P^{M+}_{\mu\nu} + A_{M-} P^{M-}_{\mu\nu} + \tilde{A}_{\mu\nu}. \tag{A10}$$

If there are no other preferred directions that enter into $\tilde{A}_{\mu\nu}$ (which is the case with the polarization tensors as long as the distribution function is isotropic), we have

$$\tilde{A}_{\mu\nu} = A_{T+} P^{T+}_{\mu\nu} + A_{T-} P^{T-}_{\mu\nu}, \tag{A11}$$

since P^T is the only available transverse, symmetric tensor and the second piece is the only anti-symmetric tensor that can be made from the Levi-Civita tensor. They can be recovered using

$$\begin{aligned}
A_Q &= P^{\mu\nu}_Q A_{\mu\nu} && \text{(A12)}\\
A_L &= P^{\mu\nu}_L A_{\mu\nu} && \text{(A13)}\\
A_{M+} &= -\frac{1}{2} P^{\mu\nu}_{M+} A_{\mu\nu} && \text{(A14)}\\
A_{M-} &= -\frac{1}{2} P^{\mu\nu}_{M-} A_{\mu\nu} && \text{(A15)}\\
A_{T+} &= \frac{1}{2} P^{\mu\nu}_{T+} A_{\mu\nu} = -A_{22} && \text{(A16)}\\
A_{T-} &= \frac{1}{2} P^{\mu\nu}_{T-} A_{\mu\nu}. && \text{(A17)}
\end{aligned}$$

The last relation on the second to last line holds when n_μ and q_μ are in the 0-3 plane.

Appendix B: Spin Sums in RMF Theory

Here we derive the spin sums of Dirac spinors essential in defining the nucleon propagators in mean field theory given earlier in Eq. 17. For Walecka type field theories, we generally have a Lagrangian of the the form

$$\mathcal{L} = \sum_B \bar{\Psi}_B (i\gamma^\mu \partial_\mu - M_B + g_{\sigma B}\sigma - g_{\omega B}\gamma^\mu \omega_\mu)\Psi_B + \mathcal{L}_{\sigma\omega} \tag{B1}$$

where we have only included a single vector field ω_μ for simplicity and the meson field self-interactions are subsumed into $\mathcal{L}_{\sigma\omega}$. The addition of isospin dependent fields to this Lagrangian is a trivial extension of the results presented below. In the mean field approximation, the scalar and vector fields behave classically and for homogeneous matter the only non-zero component of the vector field is the time component. For this Lagrangian, the equations of motion

$$\begin{aligned}
(i\gamma^\mu \partial_\mu - M_B + g_{\sigma B}\sigma - g_{\omega B}\gamma^\mu \omega_\mu)\Psi_B = 0\,, && \text{(B2)}\\
\bar{\Psi}_B(-i\gamma^\mu \overleftarrow{\partial}_\mu - M_B + g_{\sigma B}\sigma - g_{\omega B}\gamma^\mu \omega_\mu) = 0\,, && \text{(B3)}
\end{aligned}$$

are the analog of the Dirac equation in the presence of classical background fields.

First, we can find the dispersion relations nucleons by noting that fields that satisfy the Dirac equation also satisfy the Klein-Gordon equation. In standard notation, we then have

$$(i\partial\!\!\!/ - g_{\omega B}\omega\!\!\!/ - M_B^*)(-i\partial\!\!\!/ + g_{\omega B}\omega\!\!\!/ - M_B^*)\Psi_B = \left[(i\partial_\mu - g_{\omega B}\omega_\mu)(i\partial^\mu - g_{\omega B}\omega^\mu) - {M_B^*}^2\right]\Psi_B = 0 \tag{B4}$$

which admits plane wave solutions $\Psi_B \propto \exp(\mp ip\cdot x)$, and the dispersion relation is given by the equation for p^μ

$$(p_\mu \mp g_{\omega B}\omega_\mu)(p^\mu \mp g_{\omega B}\omega^\mu) - {M_B^*}^2 = 0. \tag{B5}$$

Similar to the free field case, the upper sign will correspond to particle while the lower sign will correspond to anti-particles and from now on we will only consider the particles. The equation for $\bar{\Psi}_B$ gives a similar result and if we define the four-vector

$$\tilde{p}^\mu = p_\mu - g_{\omega B}\omega^\mu = (E^*, -\vec{p}), \tag{B6}$$

the mean field theory will look almost exactly like the free field theory, just with the replacement $p^\mu \to \tilde{p}^\mu$ everywhere except for in the exponent. Here $E^* = \sqrt{p^2 + {M_B^*}^2}$ is the kinetic energy of the particle.

With this spatial dependence, we can expand the baryon fields in terms of Fourier modes and promote the expansion coefficients to creation and annihilation operators a_s and b_s and the standard four-component spinners u_s and v_s as

$$\Psi_B(x) = \sum_{s=+,-} \int \frac{d^3p}{(2\pi)^3 2E_p^*} \left(a_s(\vec{p}) u_s(\vec{p}) e^{-ip\cdot x} + b_s^\dagger(\vec{p}) v_s(\vec{p}) e^{ip\cdot x} \right) \tag{B7}$$

$$\bar{\Psi}_B(x) = \sum_{s=+,-} \int \frac{d^3p}{(2\pi)^3 2E_p^*} \left(a_s^\dagger(\vec{p}) \bar{u}_s(\vec{p}) e^{ip\cdot x} + b_s(\vec{p}) \bar{v}_s(\vec{p}) e^{-ip\cdot x} \right). \tag{B8}$$

Enforcing the standard anti-commutation relations on the fields gives

$$\left\{ a_s^\dagger(\vec{p}), a_{s'}(\vec{p}') \right\} = (2\pi)^3 \delta^{(3)}(\vec{p} - \vec{p}') 2E_p^* \delta_{ss'}, \tag{B9}$$

where the E_p^* normalization is consistent with the denominator of the Lorentz invariant phase space factor in the field expansions.

It is easy to show that the Hamiltonian density is

$$\mathcal{H} = \bar{\Psi}_B \left(i\gamma^j \partial_j + m + g\not{\omega} \right) \Psi_B. \tag{B10}$$

Integrating over space and using the field expansions gives the Hamiltonian

$$H = \sum_s \int \frac{d^3p}{(2\pi)^3 2E_p^*} \left[E_p^* a_{p,s}^\dagger a_{p',s'} \right] + g\omega_0 Q + \text{anti-particles}, \tag{B11}$$

where

$$Q = \int \frac{d^3p}{(2\pi)^3 2E_p^*} \left[a_{p,s}^\dagger a_{p',s'} \right] - \text{anti-particles}, \tag{B12}$$

is the baryon number. This result is useful when considering the grand canonical Hamiltonian, which gets also gets a contribution $-\mu Q$.

We also need to know how the presence of mean fields impacts the properties of the four-component spinors. Using the field equation for the baryon fields with the above expansions results in

$$(\not{p} - M_* - g_{\omega B}\not{\omega}) u_s(\vec{p}) = 0 \tag{B13}$$

$$\bar{u}_s(\vec{p}) (\not{p} - M_* - g_{\omega B}\not{\omega}) = 0 \tag{B14}$$

$$(-\not{p} - M_* - g_{\omega B}\not{\omega}) v_s(\vec{p}) = 0 \tag{B15}$$

$$\bar{v}_s(\vec{p}) (-\not{p} - M_* - g_{\omega B}\not{\omega}) = 0 \tag{B16}$$

The equations for $u_s(\vec{p})$ can be expressed in terms of $\tilde{p}^\mu$, in which case they take the free field form. This allows us to write down the spin sums

$$\sum_{s=\pm} \bar{u}_s(\vec{p}) u_s(\vec{p}) = \not{\tilde{p}} + M_* \tag{B17}$$

$$\sum_{s=\pm} \bar{v}_s(\vec{p}) v_s(\vec{p}) = \not{\tilde{p}} - M_*, \tag{B18}$$

which appear in the mean field propagator. Additionally, this implies that the Gordon identities and other properties of the spinors are unaltered from the free field case aside from the aforementioned replacement.

We emphasize that the above analysis dealt only explicitly with particle states. The anti-particles get a potential energy with the opposite sign from the mean field, so that the anti-particle kinetic four-momentum is given by $\tilde{p}_\mu = p_\mu + q\omega_\mu$.

Appendix C: Matsubara Sums

Here, we calculate the types of Matsubara sums necessary to evaluate the imaginary time polarization tensor. It is easiest to consider the Matsubara sums directly. Using standard methods [e.g. 33], it is easy to show that

$$T\sum_n g(i\omega_n+\alpha)=\sum \mathrm{Res}\, g(p_0)f(p_0-\alpha), \tag{C1}$$

where g is an arbitrary function of a complex variable that converges more rapidly than $1/|p_0|$ in all directions (otherwise it is necessary to be careful about which convergence factor is chosen). The pair bubble will require evaluating Matsubara sums of the form

$$\begin{aligned} S^{l,j}(i\omega_m+\Delta\mu) &= T\sum_n (i\omega_n+\nu_1)^l(-i(\omega_m-\omega_n)+\nu_2)^j \\ &\quad\times\Delta(i\omega_n+\nu_1,E_1)\Delta(i(\omega_m+\omega_n)+\nu_2,E_2), \end{aligned} \tag{C2}$$

where $\Delta(i\omega,E)=1/(\omega^2+E_p^2)$ and $E_i=\sqrt{p_i^2+m_i^2}$. We choose the energy of a particle of species 2 (rather than an anti-particle), since we will primarily be interested in the particle-particle contribution to the polarization. This results in a g of the form

$$g(p_0)=\frac{p_0^l(p_0-\omega_0)^j}{[E_1^2-p_0^2][E_2^2-(\omega_0-p_0)^2]}=\frac{p_0^l(p_0-\omega_0)^j}{(E_1+p_0)(E_1-p_0)(E_2+\omega_0-p_0)(E_2-\omega_0+p_0)}, \tag{C3}$$

where $\omega_0=-i\omega_m+\Delta\nu$ and ω_m is a Bosonic frequency. The relations

$$\frac{1}{(a+b)(a-b)}=\frac{1}{2a}\left[\frac{1}{a-b}+\frac{1}{a+b}\right]=\frac{1}{2b}\left[\frac{1}{a-b}-\frac{1}{a+b}\right] \tag{C4}$$

help define the properties of the poles found in g. The g function has four simple poles. Using the notation of equation C4, we find.

1. $p_0=E_1$, $a=E_2$, and $b=E_1-\omega_0$

$$\mathrm{Res}\, g(E_1)f = -\frac{E_1^l(E_1-\omega_0)^j}{4E_1E_2}\left[\frac{f(E_1-\nu_1)}{\omega_0-E_1+E_2}-\frac{f(E_1-\nu_1)}{\omega_0-E_1-E_2}\right]$$

2. $p_0=-E_1$, $a=E_2$, and $b=E_1+\omega_0$

$$\mathrm{Res}\, g(-E_1)f = -\frac{(-E_1)^l(-\omega_0-E_1)^j}{4E_1E_2}\left[\frac{1-f(E_1+\nu_1)}{\omega_0+E_1-E_2}-\frac{1-f(E_1+\nu_1)}{\omega_0+E_1+E_2}\right]$$

3. $p_0=\omega_0+E_2$, $a=E_1$, and $b=E_2+\omega_0$

$$\mathrm{Res}\, g(\omega_0+E_2)f = -\frac{(\omega_0+E_2)^lE_2^j}{4E_1E_2}\left[-\frac{f(E_2-\nu_2)}{\omega_0-E_1+E_2}+\frac{f(E_2-\nu_2)}{\omega_0+E_1+E_2}\right]$$

4. $p_0=\omega_0-E_2$, $a=E_1$, and $b=E_2-\omega_0$

$$\mathrm{Res}\, g(\omega_0-E_2)f = \frac{(-E_2+\omega_0)^l(-E_2)^j}{4E_1E_2}\left[\frac{1-f(E_2+\nu_2)}{\omega_0+E_1-E_2}-\frac{1-f(E_2+\nu_2)}{\omega_0-E_1-E_2}\right]$$

Combining terms that have the same denominators and carefully accounting for signs, we then have (for $l,j=\{0,1\}$)

$$\begin{aligned} S^{l,j}(i\omega_m+\Delta\mu) &= -\frac{E_1^lE_2^j}{4E_1E_2}\left[\frac{f_1(E_1)-f_2(E_2)}{-i\omega_m+\Delta\nu-E_1+E_2}+(-1)^j\frac{1-f_1(E_1)-\bar{f}_2(E_2)}{-i\omega_m+\Delta\nu-E_1-E_2}\right. \\ &\quad\left.-(-1)^{l+j}\frac{\bar{f}_1(E_1)-\bar{f}_2(E_2)}{-i\omega_m+\Delta\nu+E_1-E_2}-(-1)^l\frac{1-\bar{f}_1(E_1)-f_2(E_2)}{-i\omega_m+\Delta\nu+E_1+E_2}\right], \end{aligned} \tag{C5}$$

where $f_i(E)=[\exp(\beta E-\beta\nu_i)+1]^{-1}$.

[1] J. A. Pons, S. Reddy, M. Prakash, J. M. Lattimer, and J. A. Miralles, ApJ **513**, 780 (1999), astro-ph/9807040.
[2] L. Hüdepohl, B. Müller, H.-T. Janka, A. Marek, and G. G. Raffelt, Physical Review Letters **104**, 251101 (2010), 0912.0260.
[3] H.-T. Janka, T. Melson, and A. Summa, Annual Review of Nuclear and Particle Science **66**, 341 (2016), 1602.05576.
[4] S. Wanajo, Y. Sekiguchi, N. Nishimura, K. Kiuchi, K. Kyutoku, and M. Shibata, ApJL **789**, L39 (2014), 1402.7317.
[5] D. Radice, F. Galeazzi, J. Lippuner, L. F. Roberts, C. D. Ott, and L. Rezzolla, Mon. Not. Roy. Astron. Soc. **460**, 3255 (2016), 1601.02426.
[6] T. Melson, H.-T. Janka, R. Bollig, F. Hanke, A. Marek, and B. Müller, ApJL **808**, L42 (2015), 1504.07631.
[7] A. Burrows, D. Vartanyan, J. C. Dolence, M. A. Skinner, and D. Radice, ArXiv e-prints (2016), 1611.05859.
[8] C. J. Horowitz, O. L. Caballero, Z. Lin, E. O'Connor, and A. Schwenk, ArXiv e-prints (2016), 1611.05140.
[9] L. F. Roberts, C. D. Ott, R. Haas, E. P. O'Connor, P. Diener, and E. Schnetter, ApJ **831**, 98 (2016), 1604.07848.
[10] S. Reddy, M. Prakash, and J. M. Lattimer, Phys. Rev. D **58**, 013009 (1998), arXiv:astro-ph/9710115.
[11] G. Martínez-Pinedo, T. Fischer, A. Lohs, and L. Huther, Physical Review Letters **109**, 251104 (2012), 1205.2793.
[12] L. F. Roberts, ApJ **755**, 126 (2012), 1205.3228.
[13] L. F. Roberts, S. Reddy, and G. Shen, Phys. Rev. C **86**, 065803 (2012), 1205.4066.
[14] C. J. Horowitz, G. Shen, E. O'Connor, and C. D. Ott, Phys. Rev. C **86**, 065806 (2012), 1209.3173.
[15] E. Rrapaj, J. W. Holt, A. Bartl, S. Reddy, and A. Schwenk, Phys. Rev. C **91**, 035806 (2015), 1408.3368.
[16] R. F. Sawyer, Phys. Rev. D **11**, 2740 (1975).
[17] N. Iwamoto and C. J. Pethick, Phys. Rev. D **25**, 313 (1982).
[18] C. J. Horowitz and K. Wehrberger, Physics Letters B **266**, 236 (1991).
[19] A. Burrows and R. F. Sawyer, Phys. Rev. C **58**, 554 (1998), arXiv:astro-ph/9801082.
[20] S. Reddy, M. Prakash, J. M. Lattimer, and J. A. Pons, Phys. Rev. C **59**, 2888 (1999), astro-ph/9811294.
[21] A. Burrows and R. F. Sawyer, Phys. Rev. C **59**, 510 (1999), astro-ph/9804264.
[22] C. J. Horowitz and M. A. Pérez-García, Phys. Rev. C **68**, 025803 (2003), arXiv:astro-ph/0305138.
[23] L. F. Roberts, G. Shen, V. Cirigliano, J. A. Pons, S. Reddy, and S. E. Woosley, Phys. Rev. Lett. **108**, 061103 (2012).
[24] G. I. Lykasov, C. J. Pethick, and A. Schwenk, Phys. Rev. C **78**, 045803 (2008).
[25] S. Reddy, G. Bertsch, and M. Prakash, Physics Letters B **475**, 1 (2000), nucl-th/9909040.
[26] H. Sonoda, G. Watanabe, K. Sato, T. Takiwaki, K. Yasuoka, and T. Ebisuzaki, Phys. Rev. C **75**, 042801 (2007), astro-ph/0701364.
[27] C. J. Horowitz, D. K. Berry, M. E. Caplan, T. Fischer, Z. Lin, W. G. Newton, E. O'Connor, and L. F. Roberts, ArXiv e-prints (2016), 1611.10226.
[28] L. B. Leinson and A. Perez, Phys. Lett. **B518**, 15 (2001), [Erratum: Phys. Lett.B522,358(2001)], hep-ph/0110207.
[29] C. J. Horowitz, Phys. Rev. D **65**, 043001 (2002), arXiv:astro-ph/0109209.
[30] A. L. Fetter and J. D. Walecka, *Quantum theory of many-particle systems* (1971).
[31] R. Kubo, Journal of the Physical Society of Japan **12**, 570 (1957).
[32] L. D. Landau and E. M. Lifshitz, *Statistical physics. Pt.1, Pt.2* (1980).
[33] M. Le Bellac, *Thermal Field Theory* (2000).
[34] K. Takahashi, M. F. El Eid, and W. Hillebrandt, A&A **67**, 185 (1978).
[35] R. Mertig, M. Böhm, and A. Denner, Computer Physics Communications **64**, 345 (1991).
[36] C. Giunti and W. K. Chung, *Fundamentals of Neutrino Physics and Astrophysics* (Oxford University Press, 2007).
[37] S. W. Bruenn, ApJS **58**, 771 (1985).
[38] B.-A. Li and L.-W. Chen, Modern Physics Letters A **30**, 1530010 (2015), 1503.00370.